Single-cell transcriptomic analysis deciphers key transitional signatures associated with oncogenic evolution in human intramucosal esophageal squamous cell carcinoma

Xin-Yang Liu
Endoscopy Center and Endoscopy Research Institute, Zhongshan Hospital, Fudan University, Shanghai
Yan-Bo Liu
Endoscopy Center and Endoscopy Research Institute, Zhongshan Hospital, Fudan University, Shanghai
Jia-Cheng Xu
Endoscopy Center and Endoscopy Research Institute, Zhongshan Hospital, Fudan University, Shanghai
Yi-Fei Zhang
Endoscopy Center and Endoscopy Research Institute, Zhongshan Hospital, Fudan University, Shanghai
Yuan-Yuan Ruan
Department of Biochemistry and Molecular Biology, School of Basic Medical Sciences, Fudan University,No.130 Dongan Road, Shanghai
Yi Zhao
GobioX BioTech, Shanghai
Lin-Feng Wu
Endoscopy Center and Endoscopy Research Institute, Zhongshan Hospital, Fudan University, Shanghai
Jian-Wei Hu
Endoscopy Center and Endoscopy Research Institute, Zhongshan Hospital, Fudan University, Shanghai
Zhen Zhang
Endoscopy Center and Endoscopy Research Institute, Zhongshan Hospital, Fudan University, Shanghai
Meng-Jiang He
Endoscopy Center and Endoscopy Research Institute, Zhongshan Hospital, Fudan University, Shanghai
Tian-Yin Chen
Endoscopy Center and Endoscopy Research Institute, Zhongshan Hospital, Fudan University, Shanghai
Xiao-Yue Xu
Endoscopy Center and Endoscopy Research Institute, Zhongshan Hospital, Fudan University, Shanghai
Jing-Wei Zhang
State Key Laboratory of Genetic Engineering, School of Life Sciences, Fudan University, Shanghai
Yi-Qun Zhang
Endoscopy Center and Endoscopy Research Institute, Zhongshan Hospital, Fudan University, Shanghai
Ping-Hong Zhou (zhou.pinghong@zs-hospital.sh.cn)

Endoscopy Center and Endoscopy Research Institute, Zhongshan Hospital, Fudan University, Shanghai

Research Article

Keywords: Esophageal squamous cell carcinoma, Intramucosal, Single-cell RNA-seq, Tumor microenvironment, Heterogeneity

Posted Date: May 10th, 2022

DOI: https://doi.org/10.21203/rs.3.rs-1608801/v1

Abstract

Background: The early diagnosis and intervention of esophageal squamous cell carcinoma (ESCC) is particularly important due to poor prognosis and the lack of effective therapies. This study aims to systematically describe the cellular atlas of human intramucosal ESCC.

Methods: Five paired samples of intramucosal ESCC, para-ESCC esophageal tissue from endoscopically resected specimen, and peripheral blood mononuclear cells were adopted for scRNA-seq analysis. A computational pipeline scMetabolism was applied to quantify the metabolic diversity of single cells.

Results: A total of 164,715 cells were profiled. The abundance of CD8+ TEXs , Tregs and PD1+CD4+T cells suggested an exhausted and suppressive immune microenvironment. Several genes in immune cells such as CXCL13 and CXCR5 in PD1+CD4+ T cells and PADI4 in Mono2 cells were identified as new biomarkers for poor prognosis. Epithelial cells exhibited high intra-tumor heterogeneity and two evolutional trajectories during ESCC tumorigenesis initiated from proliferative cells, and then through an intermediate state, to two different terminal states of normal differentiated epithelial cells or malignant cells, respectively. Intercellular interaction analysis based on ligand-receptor pairs revealed malignant cells interacting with CAFs via the MDK-NCL pathway, which is an important hallmark in the change of tumor microenvironment, and serves as a sign of CAF activation to stimulate downstream pathways for facilitating tumor invasion, and therefore suggesting a potential early biomarker of ESCC progression.

Conclusions: This study demonstrates the changes of cell subsets and transcriptional levels in human intramucosal ESCC, providing unique insights into the development of novel biomarkers and potential intervention strategies.

Background

Esophageal squamous cell carcinoma (ESCC) is one of the most common and deadly gastrointestinal malignancies. The situation is especially prominent in Asia[1, 2]. Compared with surgery, endoscopic resection and endoscopic ablation such as photodynamic therapy, cryotherapy and radiofrequency ablation could be applied to early ESCC confined to esophageal mucosal and submucosal layers, with comparative efficacy but less complications[3]. In advanced ESCC, more than 50% of patients might not be eligible for surgery upon diagnosis. Even in patients who have received surgery, the 5-year metastasis and recurrence rate is still more than 40%, and the 5-year survival rate could not reach 25%[4]. Currently, there has been limited progress in target therapy and immunotherapy[5, 6]. Therefore, the early diagnosis and intervention of ESCC is particularly important.

ESCC undergoes a sequence of development from inflammation, hyperplasia, dysplasia, carcinoma in situ, to invasive carcinoma. Exploring the underlying mechanisms of ESCC initiation and development is extremely important to early detection and precision treatment. Recent whole-exome or whole-genome sequencing studies have identified many genomic variations in ESCC[7], howevertraditional sequencing

studies have obtained the overall average characteristics of cell populations, where the characteristics of the dominant cell population are more likely to be explicit, while the rare low abundance characteristics are often drowned in a vast number of bulk signals. For the tumor microenvironment ecosystem formed by spatio-temporal interaction, single cell transcriptome sequencing provides a promising tool for deeper analysis of a variety of heterogeneous cells, including malignant cells, immune cells and stromal cells. Using such novel technique, immune suppressive microenvironment in human progressive ESCC has been described that may be responsible for the failure of immuno-surveillance[8]. A set of key transitional signatures associated with oncogenic evolution of epithelial cells and a chronic inflammatory environment that promotes carcinogen-transformed epithelial cell survival and proliferation was also observed in a mouse model mimicking human ESCC development[9]. Due to the high quality of fresh specimen needed and the scarcity of tissue obtained from endoscopic resection, there is no comprehensive study on the tumor ecosystem of early ESCC at the single cell level yet.

In order to understand the tumor ecosystem of intramucosal ESCC, 5 patients with Tis and T1a stage ESCC were collected. This study aims to systematically describe the transcriptome landscape of intramucosal ESCC and to clarify the changes of cell subsets and transcriptional levels related to pathogenesis of early ESCC in the tumor microenvironment, which will provide evidence for development of novel biomarkers and insights for the early intervention or reversal of ESCC.

Methods

Patients

For scRNA-seq, 5 patients clinically diagnosed with Tis and T1a stage ESCC were collected from the Department of Endoscopy, Zhongshan Hospital, Fudan University. Specimens from endoscopic submucosal resection (ESD) were stained with Lugo’s iodine for classification of unstained tumor tissue and deeply stained paratumor epithelial mucosa[10, 11]. A 1mm*1mm sample from the lesion and a 1mm*1mm sample from the paratumor area was taken from each resected specimen in order to minimize the influence on pathological assessment. Peripheral blood mononuclear cells (PBMC) from each patient were also collected. Final pathological diagnosis was confirmed by evaluating the ESD resected specimen. Patients were excluded if the pathological diagnosis did not meet the standard of Tis or T1a stage. Another 15 surgically resected ESCC samples at different stages were included for immunohistochemistry.

Tissue dissociation and cell purification

Tissues were transported in sterile culture dish with 10 ml 1x Dulbecco's Phosphate-Buffered Saline (DPBS; Thermo Fisher) on ice to remove the residual tissue storage solution, then minced on ice. Intramucosal ESCC and paratumor tissues were dissociated in 0.1% collagenase IV digestive solution (RPMI-1640 medium (Invitrogen) with 10% Fetal Bovine Serum (FBS; Thermo Fisher) containing collagenase IV (Sigma)) at 37 ℃ with a shaking speed of 50 r.p.m for about 40 min. Cell suspensions

were filtered using a 40-μm nylon cell strainer and red blood cells were removed by 1X Red Blood Cell Lysis Solution (Thermo Fisher). Dissociated cells were washed with 1 X DPBS containing 2% FBS. Cells were stained with 0.4% Trypan blue (Thermo Fisher) to check the viability on Countess® II Automated Cell Counter(Thermo Fisher). Peripheral blood mononuclear cells (PBMC) were isolated using lymphocyte-h (lymphocyte isolation solution, Cedarlane) and red blood cell lysis solution(Thermo Fisher) according to the manufacturer's instructions. Lymphocytic cells was washed twice with DPBS and resuspended with sorting buffer.

Single cell RNA sequecing

Following tissue digestion, samples were sequenced by 10 X Chromium single cell platform (10 X Genomics, 30 v3 chemistry, Rev C). In detail, Gel bead in EMulsion (GEM) were generated and mRNAs from single cells were then subject to second-strand cDNA synthesis, adaptor ligation, and universal amplification was performed. Then, all the remaining procedures including the library construction were performed according to the standard manufacturer's protocol (CG000206 RevD). The libraries were sequenced on NovaSeq6000 (Illumina). Single cell RNA-seq data processing reads, alignment, and initial clustering of the raw scRNA-seq profiles were progressive using the Cell Ranger 3.0.1 pipeline with default and recommended parameters.

Data analysis

This output was then imported into the Seurat (4.0.1) R toolkit for quality control and downstream analysis of our scRNA-seq data. All functions were run with default parameters, unless specified otherwise. We excluded cells with fewer than 200 or more than 6000 detected genes (where each gene had to have at least one UMI aligned in at least three cells). The expression of mitochondria genes was calculated using PercentageFeatureSet function of the Seurat package. To remove low activity cells, cells with more than 10 percent expression of mitochondria genes were excluded. The normalized data (NormalizeData function in Seurat package) was performed for extracting a subset of variable genes. Variable genes were identified while controlling for the strong relationship between variability and average expression. Next, we integrated data from different samples after identifying 'anchors' between datasets using FindIntegrationAnchors and IntegrateData in the seurat package. Then we performed principal component analysis (PCA) and reduced the data to the top 30 PCA components after scaled the data. We visualized the clusters on a 2D map produced with t-distributed stochastic neighbor embedding (t-SNE). For sub-clustering, we applied the same procedure of scaled, dimensionality reduction, and clustering to the specific set of data (usually restricted to one type of cell.) For each cluster, we used the Wilcoxon Rank-Sum Test to find significant deferentially expressed genes comparing the remaining clusters. Cells with mix features were removed from further analysis. Clusters were identified using FindClusters function, and the specific gene markers for each cluster were determined using the FindAllMarkers function implanted in Seurat package.

Estimation of the copy number variations and cell developmental trajectory

The R package “infercnv”[12] was used to estimate the initial copy number variations (CNVs) in each region. The expression level of each cell acted as the input file with recommendatory parameters. Immune cells served as the background to calculate the CNVs score. The CNV value of each cell was calculated as the quadratic sum of the CNV region[13, 14]. The cell lineage trajectory of epithelial cells was inferred by using Slingshot(proposed by Street et al. 2017).

Analyses of metabolic pathways

A recently developed computational pipeline for quantifying single-cell metabolism, scMetabolism(v0.2.1), was also applied for visualization and quantifying the metabolic diversity of single cells in each cluster[15].

Functional enrichment analyses

Gene Ontology (GO) and Kyoto Encyclopedia of Genes and Genomes (KEGG) pathway analyses were performed via clusterProfiler(3.18.1)[16], GSVA(1.38.2), and GSEABase(1.52.1).

Construction of a cell to cell interaction network

To investigate cell-to-cell interaction among T cells, CAFs and epithelial cells, R package “CellChat” (1.1.2)[17] was applied. The ligand-receptor pairs in CellChat were retrieved from previous studies[18].

GEPIA (Gene Expression Profiling Interactive Analysis) dataset

GEPIA(a web server for cancer and normal gene expression profiling and interactive analyses) uses standard processing pipelines to analyze the RNA sequencing expression data from 9,736 tumors and 8,587 normal samples from the TCGA and GTEx projects., providing customizable features such as correlation analysis, tumor / normal differential expression analysis, similar gene detection, and patient survival analysis.

Immunohistochemistry

Immunohistochemistry (IHC) was performed in ESCC specimen of paratumor tissue, high grade dysplasia, intramucosal ESCC and progressive ESCC. Samples were used for staining of LUM (Cat#ab168348, Abcam) NCL (Cat# ab129200, Abcam) and MDK (Cat# ab52637, Abcam) antibodies.

Statistical analyses

Cell distribution comparisons between two groups were performed using unpaired two-tailed Wilcoxon rank-sum tests. Comparisons of gene expression or gene signature between two groups of cells were performed using unpaired two-tailed Student’s t test. All statistical analyses and presentation were performed using R and statistical significance was set at $p < 0.05$.

Results

A scRNA-Seq census of human intramucosal ESCC identifies 12 distinct cell populations and differentiation relations

To create a comprehensive single-cell landscape of human intramucosal ESCC, we applied scRNA-seq using paired samples of endoscopically resected intramucosal ESCC, para-ESCC esophageal tissue from endoscopically resected specimen, and PBMC. Intramucosal ESCC lesion and para-ESCC esophageal tissue were identified using iodine staining on the endoscopically resected specimen. Namely, the non-staining area indicated early ESCC whereas deep-staining area represented non-ESCC paratumor tissue, respectively. A 1mm*1mm sample from the lesion and a 1mm*1mm sample from the paratumor area was taken from each resected specimen in order to minimize the influence on pathological assessment (Fig. 1A). Five pairs of samples were included after pathological confirmation, and demographic data indicated in Table 1. After quality control to remove low-quality cells, a total of 16,4715 cells were retained for further analyses. Among them, 48,711 cells derived from intramucosal ESCC samples (6736 ~ 11794, median: 9912/patient), 55,191 cells derived from paratumor samples (8417 ~ 13876, median: 10127/patient), and 60,813 cells derived from PBMC (10422 ~ 14256, median: 11951/patient). A median of 1634 genes per cell was detected.

Table 1
Demographic and pathological characteristics of patients.

	Age	Sex	Tissue size(cm)	Iodine uncolored area(cm)	Microscopic lesion(cm)	Stage (depth of tumor invasion)
Patient01	55	Male	3*2.5	2.5*1.5	3*2	T1a (Muscularis mucosae)
Patient02	65	Female	3.8*2.3	2.5*1.3	3*l.2	T1a (Lamina propria mucosa)
Patient03	72	Male	3.9*5	2.7*2	3*2.5	Tis
Patient04	75	Male	9*8	8*7	4.8*4.3	T1a (Lamina propria mucosa)
Patient05	68	Male	5.8*2.8	5.2*2.2	4.8*1.5	T1a (Lamina propria mucosa)

Based on the expressions of canonical markers, we classified cells into 12 clusers by using t-distributed stochastic neighbor embedding (tSNE) (Fig. 1B), including megakaryocyte cells, cancer-associated fibroblasts (CAFs), dendritic cells, plasma cells, endothelial cells, myofibroblasts, proliferating cells, B cells, T cells, monocytes, epithelial cells, and natural killer (NK) cells. Marker genes of the identified 12 major cell types were cell type specific and consistent with classic, well-established markers for each respective cell population. (Fig. 1C, Supplementary Figure S1A).

Noteably, the proportion of immune cells in the tumor tissue increased significantly compared with the paratumor tissue, such as B and T cells. In contrast, epithelial cells are the dominant cluster in the paratumor tissue (Fig. 1D). What's more, an increase in B cell proportion was observed in both the tumor and paratumor tissues from patient 3 (Fig. 1E), who was identified as high-grade intraepithelial neoplasia rather than carcinoma in situ (Table 1). In intramucosal ESCC, the average proportion of infiltrating B cells was significantly higher than that in the progressive ESCC[8] (Fig. 1F). However, a decrease in the proportion of infiltrating B cells in progressive ESCC compared to other cancer types was reported in previous studies[19], indicating the positive effects of tumor-infiltrating B cells.

Transcriptomic inter-tumor heterogeneity and transitional cell status of epithelial cells in human intramucosal ESCC

To investigate how normal esophageal epithelium develops into carcinoma, various tools were introduced to assess the genetic alterations and functional changes in epithelial cells harvested from tumor and paratumor tissues. A total of 28397 epithelial cells were identified and were classified into 7 subclusters designated as E1 ~ E7, and the tSNE plot revealed the subcluster distribution among sample pathology (Fig. 2A). E6 ~ E7 was enriched in tumor samples, while a higher fraction of E1, E2 and E3 clusters was observed in paratumor samples (Fig. 2B,C). GO terms were enriched in normal epithelial function such as epidemis development and cornification in E1, E2 and E3 subclusters. E4 was enriched in ATP metabolic process, and E5 ~ E7 were enriched in protein folding and RNA splicing (Fig. 2D). Although there was no distinct difference in gene expression profile across cell subclusters, a gradual increase in the expression level of oncogenes with a gradual decrease in tumor supressors could be identified. For example, TMPRSS11B, MUC21, CRNN were highly expressed in the upper right corner of the tSNE plot characterized by E1 subcluster, while the expression of SOX4, MDK and IFI6 was higher in the upper left corner characterized by E6 and E7 subclusters (Fig. 2E). DSC2, RT4 and IL1RN were highly expressed in subclusters other than E6 or E7 (Supplementary Figure S1B). Interestingly, when assessing the proportion of epithelial cells that contributed to each cluster by each patient sample, we found that E7 subcluster did not present in patient 03 (Fig. 2F). Moreover, the pathological diagnosis of this patient was high grade intraepithelial neoplasia, while all the others were carcinoma. This finding further confirmed the hypothesis of E7 as a subcluster of malignant cells. What's more, the proportion of E7 also demonstrated positive correlations with an increase in the depth of tumor invasion (Supplementary Table S1) rather than the size of microscopic lesion, indicating the potential relationship between E7 and tumor invasion. Notably, the suggested malignant E7 subcluster and potentially malignant E4, E5 and E6 subclusters also presented in paratumor tissues(Supplementary Figure S2B). These results suggested the paratumor tissues may have shared an extensive overlap with intramucosal ESCC.

CNV analysis of epithelial cells was performed and Bayes normalization was applied (Fig. 2G, Supplementary results). Epithelial cells originated from tumor tissues exhibited a relative variation in CNV profiles compared to epithelial cells originated from paratumor tissues(Supplementary Figure S2A). E1 subcluster showed lower variation in CNV compared to other subclusters, suggesting the benign nature of

this subcluster. The CNV signal at the anterior end of chromosome 6 was highest in E7 subcluster and also increased in E5 and E6 subclusters. E7 subcluster exhibited a unique gain in CNV at the posterior end of chromosome 20 and the middle of chromosome 3.

We then performed pseudotemporal and PCA analysis and found two evolution fates of esophageal epithelial cells during ESCC tumorigenesis initiated from proliferative Epi4, and then through an intermediate state characterized by E5, to two different ternimal states of normal differentiated E1/E2/E4 or malignant E6/E7, respectively (Fig. 2H). This is also similar to the previously reported cell fates of epithelial cell status transitions in mouse ESCC model[9]. Besides, expression of several genes of E7 sphingolipid metabolism changed along the trajectory (Fig. 2I).

Metabolic characteristics of epithelial cells in human intramucosal ESCC

Aberrant metabolism is a major hallmark of cancer. Abnormal cancer metabolism, such as aerobic glycolysis and increased anabolic pathways, plays an important role in tumorigenesis, metastasis, drug resistance, and cancer stem cells[20].

To understand the metabolic landscape of epithelial cells in intramucosal ESCC, we first computed the score of all 76 active metabolic pathways in all E1-E7 clusters and selected 24 representing metabolic pathways by using the scMetabolism[15]. We found significant metabolic change trend from E1 to E7. E7(a group of characteristic cells prone to malignancy) showed significantly different characteristics compared with other epithelial cell clusters.

The level of glycolysis, pyruvate metabolism, oxidative phosphorylation, amino acid metabolism (e.g., Tyrosine metabolism) and lipid metabolism (e.g., Steroid biosynthesis) were lower in E7 than other epithelial clusters (Fig. 2J), which is different from progressive cancer [21]. Similar to the progressive ESCC, a distinct increase in glycan biosynthesis and metabolism(e.g., Glycosaminoglycan degradation /biosynthesis, other types of O − glycan biosynthesis) was observed in E7.

In order to explore the relationship between E7 and tumor progression, we analyzed the correlationship between the representing metabolic pathaways and tumor phenotypes by computing the classical phenotypic scores of cancer cells(Fig. 2K). Through the correlation of phenotypic score and metabolic pathways, we found that markers of E7 were strongly associated with metastasis and angiogenesis, which is not significant in other phenotypes such as cell proliferation.

Sphingolipid metabolism and glycan biosynthesis/metabolism(e.g., glycosaminoglycan degradation /biosynthesis) showed strong positive correlation with both metastasis and angiogenesis, which is consistent with previous studies[22]. We further found marker genes such as KDSR, DESG1,PLPP1 and NEU1 after searching for the marker genes related to sphingolipid metabolism in E7. The expression of KDSR was increased along the malignant trajectory, and NEU1 were significantly highlited in the E7 cells as mentioned above (Fig. 2I).. The results of PCR demonstrated that the knockdown of KDSR potentially

inhibited EMT of ESCC in vitro by observing a decrease in the expression of snail and slug at the RNA level, indicating a potential target for the development of anti-tumor strategies (Supplementary Figure S2C).

In conclusion, all the results above demonstrated that early ESCC shared both similarities and differences with progressive cancer and ehanced sphingolipid metabolism in E7 showed a strong correlationship with tumor matastasis and angiogenesis.

Exhausted T cells and suppressive immune microenvironment in human intramucosal ESCC

As the vast majority of T cells derived from PBMC, clustering of T cells were independently performed for PBMC, tumor tissues and paratumor tissues, respectively, so as to avoid losing signals from tissue samples.

For PBMC, ten clusters of T cells were characterized with distinctive signatures, namely $CD8^+$ CTL, $CD4^+$ Naïve T cells, $CD8^+$ translational T cells, $CD4^+$ T_{EM}s, γδ T cells, $CD4^+$ Cytotoxic T cells, NKT, $CD4^+$ T_{CM}s, NK-like $CD16^+$ T cells, and Tregs (Fig. 3A). For tissue samples, Four T cell clusters presented both in tumor tissues and paratumor tissues (Fig. 3B, C, Supplementary results), including Tregs, $CD8^+$ CTLs, $PD1^+CD4^+$ T cells, $CD4^+$ T_Ms (Memory T cells). Among them, $PD1^+CD4^+$ T cells has previously been reported not to be present in paratumor tissues of advanced ESCC samples[23]. T cells from tumor tissues and paratumor tissues also exclusively exhibited distinct clusters. $CD8^+$ T_Ms, MAIT (mucosal-associated invariant T) cells and $CD4^+$ T_Ns (Naïve T cells) presented in paratumor tissues while $CD8^+$ T_{EX}s (Exhausted T cells), $CD4^+ISG^+$ T cells and $CD4^+$ T_Ns only presented in tumor tissues(Fig. 3D). Additionally, it is worth noticing that CD8 + T_{EX}s expressed a high level of GZMK rather than its typical marker CXCL13, suggesting that CD8 + T_{EX}s in intramucosal ESCC tissues are mainly in an intermediate state, and might go through a 'Tn to IL7R + Tm to GZMK + $T_{EM/EX}$' pathway to become terminal T_{EX} [24]. Notebly, The proportions of T cell clusters in paratumor tissues in one of the patient 03 was significantly different from other patients, with a higher proportion of $CD4^+$ T_Ms, $PD1^+CD4^+$ T cells, and MAIT cells, whereas a decreased proportion of $CD8^+$ T_Ms (Supplementary Figure S3B).

Taken together, the abundance of CD8 + T_{EX}s and enrichment of Tregs and PD1 + CD4 + T cells suggested exhausted and suppressive immune microenvironment in human intramucosal ESCC.

Metabolic charateristics of extausted T cells in human intramucosal ESCC

Recent studies on immunometabolism have demonstrated a close connection between metabolic programing and the specific immune functions they support during both health and disease [25].

To understand the metabolic landscape of T cells in intramucosal ESCC microenvironment, we computed the score of 24 representing metabolic pathways using scMetabolism in all T clusters. We found effector T cells and exthausted T cells (cells normally marked with CD28 family inhibitory receptors), acted abnormally after activation(Fig. 3F).

Exhausted CD8 + T cells were only found in tumor. As mentioned above, exhausted CD8 T cell had a significantly lower metabolic level, including glycolysis, oxidative phosphorylation, TCA cycle, etc (Fig. 3F), which indicated the failure of activation. In contrast, the steroid biosynthesis of these cells was specifically up-regulated, which may help tumor cells escape[26]. Different from exthausted CD8 + T cells, we observed the enhancement of glycolysis/gluconeogenesis and oxidative phosphorylation in intramucosal ESCC infiltrated PD1 + CD4 + T cells, with the increase of other types of O − glycan biosynthesis, etc (Fig. 3F), indicating the tumor infiltrated PD1 + CD4 + T cells still maintained high metabolic activity, despite the expression of PD1.

To explore the association of metabolic characteristics with phenotypic changes of PD1 + CD4 + T cells, we also carried out the correlation analysis here by computing the classical phenotypic scores of T cells such as interleukin signaling pathway, antigen processing and presentation, inflammation, and immune suppression(Fig. 3G). Interestingly, interleukin signaling pathway is sigificently negatively accociated with several metabolic pathways such as glycolysis, citrate cycle (TCA cycle) and pentose phosphate pathway. It is supposed that PD1 + CD4 + T cells are more active in catabolism rather than anabolism, which makes the cytokines secreted by CD4 + T cells insufficient, resulting in abnormal immune response and inhibition of cell proliferation and growth pathway[27].

More importantly, we found that PD1 + CD4 + T cells were associated with significently more numbers in tumors compared to the adjacent tissues, and the top 20 markers of these cells in tumor tissues (logfc > 0.95, $P < 0.001$) were associated with a lower probability of overall survival in ESCC (Fig. 3H). However, there was no significant correlation between the top markers of PD1 + CD4 + T cells in adjacent tissues and the survival of esophageal cancer. Among them, we observed the specific high expression of CXCL13 and CXCR5 in PD1 + CD4 + T cells in tumor tissues (Fig. 3I).

Characterization of myeloid cell differentiation

Seven monocyte/macrophage cell clusters were categorized (Fig. 4A). Mono1(with high expression of VCAN) and Mono2(with high expression of PADI4) both showed similarity with the classical CD14 + CD16- monocytes. Classically activated macrophages (M1, Macro1, with high expression of CSF1R), alternatively activated macrophages (M2, Macro3, with high expression of ATF3), and myeloid-derived suppressor cells (MDSCs) (Fig. 4B), macrophage clusters were identified using published gene signatures of myeloid cells[8, 9]. Macro2 may represent the intermediate state, both enriched monocyte, M1 and M2 signature. Macro4 was denoted as tissue resident macrophages (TRM). Interestingly, PADI4, the marker gene of Mono2 subcluster, was strongly associated with a high probability of overall survival in ESCC (Fig. 4C), suggesting it as a prognostic biomarker in ESCC. Human PADI4 was first described in HL-60

cells and was found to participate in differentiation of HL-60 cells into granulocytes and monocytes/macrophages[28].

Eight DC clusters were characterized according to discriminative markers, including cDC1, CD1C + LYZ- DC, CD1C + LYZ + DC, pDC, cycling DC, LAMP3 + DC, S100A9 + DC, and IFN induced DC (Fig. 4D, Fig. 4E, Supplementary results). Notebly, cycling DC(subcluster in cell cycle) was enriched in tissues compared with PBMC (Fig. 4F). LAMP3 + DC was recently recognized by several studies [29–31] as a tumor-specific DC subcluster, which was the most activated DC subset with potential migration capacity in tumors. Although some of the subclusters showed different proportions in PBMC and tissues, only LAMP3 + DC was significantly different in quantity between tumor and paratumor tissues (Fig. 4F). Accordingly, LAMP3 + DC was greatly enriched in human intramucosal ESCC specimen, compared to paratumor tissues and PBMC. Among the 8 DC subgroups, LAMP3 + DCs expressed various immune-relevant genes encoding cytokines (IL7R, IL15, IL32), chemokines and chemokine receptors(CCR7, CCL19, and CCL22) (Fig. 4E,G), exhibiting potential to regulate multiple subtypes of lymphocytes[32].

Distinct fibroblast subpopulations in human intramucosal ESCC ecosystem

1,279 cancer associated fibroblasts (CAFs) were clustered into 5 subpopulations (Fig. 5A). All 5 subclusters expressed high levels of fibroblast markers such as ACTA2 (a-SMA), PDGFRa, DCN, FN1 and LUM (Fig. 5B), while each subcluster displayed distinct transcriptomic signatures(Fig. 5C, Supplementary Figure S4, Supplementary results). Interestingly, although the GO terms enriched for iCAF1 and iCAF2 have common pathways related to extracellular matrix organization and extracellular structure organization (Fig. 5D), their pathways related to inflammatory response were opposite. iCAF1 participated in the negative regulation of immune system process, while iCAF2 paricipated in complement activation and complement-dependent cytotoxicity. Therefore, the role of iCAF1 was further identified as inhibition in immune modulation and iCAF2 as activation. Moreover, iCAF1 was mainly enriched in ESCC tissues, whereas proportion of iCAF2 was relatively higher in adjacent tissues, which was also consistent with the suppressed immune status in tumorgenesis (Fig. 5E). The active metabolism of iCAF1 was featured with high level of lipid metabolism through scMetabolism(Supplementary Figure S5), including glycosphingolipid biosynthesis and glycerophospholipid metabolism. It was proposed that the ehancement of lipid metabolism of CAFs promotes tumor metastasis[33]. mCAF1 and mCAF2 expressed high levels of extracellular matrix signatures and GO terms(Fig. 5D). eCAF mainly expressed epithelium-specific marker genes and GO terms, which was in consistent with the EMT-like CAFs in a previous report [34]. ScMetabolism also displayed a significant increase in the strong metabolic activity of eCAF(Supplementary Figure S5). Therefore, we speculate that this cluster of cells may be related to the proliferation and biosynthesis of tumor related fibroblasts, and may communicate with tumors. Notably, when combining all CAF subgroups together, GO analysis showed that CAFs derived from tumor specimen manifested different pathway enrichment compared with CAFs derived from paratumor specimen(Fig. 5F). CAFs derived from tumor specimen was associated with higher signals in extracellular matrix organization, extracellular structure organization,antigen processing, and response to oxygen

levels. Previous reports have also highlighted a subcluster called vCAF in malignant tumors [34, 35], characterized by microvasculature signature genes such as CD146 (MCAM), MYH11 and RGS5, as well as inflammatory chemokines such as IL-6 and CCL8, with functions mainly in response to hypoxia and mesenchymal cell proliferation. However, this subcluster was not found in human intramucosal ESCC, which may be related to the biobehavior of this very early stage of ESCC.

E7 cells interact with CAFs via the MDK-NCL pathway

To explore the interactions among T cells, epithelial cells and CAFs, we conducted intercellular interaction analyses based on ligand-receptor pairs (Fig. 6A ~ C). Different from progressive ESCC, the interactions between different cell types decreased a lot because of the early stage of the tumor[21]. In the network of the intramucosal ESCC, interactions between the epithelial cells and CAFs were predicted to be most significant. An increasing intercellular interaction in the MDK (Midkine)-SDC2 (Syndecan-2), MDK-NCL (Nucleolin) and MDK-LRP1(LDL Receptor Related Protein 1) axis was observed between epithelial cells and CAFs, and the interactions between E7 cluster and eCAFs/iCAFs were observed to be the most prominent. In the MDK-NCL axis, E7 showed a particularly strong intercellular interaction with eCAF and mCAF2 (Fig. 6D).

Gypia database was then explored for the expression level of MDK, NCL and LRP1. The results suggested the expression level of MDK and NCL in human esophageal cancer was higher than that in paratumor tissue (Fig. 6E). In correlation analysis using data from TCGA and GTEx, the expression level of MDK was significantly correlated with NCL in human esophageal cancer and paratumor esophageal tissues(Fig. 6F). However, there was no significant difference for LRP1. We then further performed IHC in ESCC specimen of paratumor tissue, high grade dysplasia, intramucosal ESCC and progressive ESCC (Fig. 6G, Supplementary Table S2). Expectedly, with the progressing of ESCC, the expression of MDK and NCL in tumor tissue increased step by step, and the close location indicated the interaction between the CAFs and tumor.

Collectively, these results indicated that MDK was upregulated in esophageal epithelial cells during malignancy change and interacted with NCL in mCAF and eCAF to promote the proliferation of CAFs. The enriched MDK-NCL signal could serve as a sign of CAF activation to stimulate downstream pathways for facilitating tumor invasion, and therefore might be a potential early biomarker of ESCC progression .

Discussion

Here, we systematically describe the single-cell transcriptome and metabolism landscape of human intramucosal ESCC. Detection of early ESCC almost completely depends on timely gastroscopy due to the nonspecific symptoms in early ESCC. Post ESD pathological diagnosis is crucial for the confirmation of treatment adequacy and further intervention or follow-up plans. Proposing minimal influence on pathological assessment as a prerequisite, the sample volume from ESD specimen is limited, proposing scRNA-seq as one of the most appropriate methods for describing early ESCC microenvironment.

However, there is currently no transcriptome landscape description of human early ESCC on a single cell resolution .

The metabolic characteristics of intramucosal ESCC shared both similarities with and differences from progressive ESCC. The level of glycolysis, pyruvate metabolism, oxidative phosphorylation, amino acid metabolism and lipid metabolism still stayed low in E7, which is different with progressive cancer[21, 36], indicating that intramucosal ESCC may haven't started a large scale of cell growth and proliferation or suffered from nutrientand oxigendeprivation. Notebly, the proportion of E7 also demonstrated positive correlations with an increase in the depth of tumor invasion, which supported us to further explore the relationship between the metabolic changes and the invasive phenotypes. Correlation analysis suggested that sphingolipid metabolism showed a strong correlation with cancer metastasis, which is consistent with previous studies[6]. Sphingosine synthesis in sphingolipid metabolism plays an important role in the growth and metabolism of cancer cells[22]. KDSR in this pathway were found to be significantly upregulated along the trajectory, with qRT-PCR indicating a potential target for the development of anti-tumor strategies.

Our results suggested high inter-tumor heterogeneity and of epithelial cells in human intramucosal ESCC. The subclusters of epithelial cells demonstrated a transitional cell status, in which only a small portion of cells were malignant tumor cells, whereas the vast majority are still in their way of malignancy change. This finding is in line with the biological nature of early ESCC. Meanwhile, the paratumor tissues were not normal esophageal tissues, without distinct boundary with neoplasia. Considering the sampling technique of choosing unstained area in the ESD resected specimen, pre-cancerous status such as low grade intraepithelial neoplasia could also present in paratumor tissues. Actually, in clinical work, lightly stained mucosa or suspecious satellite lesions often present surrounding the major unstained lesion with pathological confirmation as the target for ESD. Our results revealed the abundance of potentially malignant cells in ESCC paratumor tissues, and might also help to explain the reason for high risk of metachronous de novo carcinogenesis. The result is also in accordance with previous findings that genomic mutations that were responsible for ESCC development might also occur in normal pathologically paratumor human esophageal tissues, and what's more, tumor-adjacent paratumor epithelia shared an extensive overlap with dysphagia[9].

It is worth noticing that the steroid biosynthesis of CD8 exhausted T cells was more active. Previous articles have shown that the helper T cells producing steroids cause the imbalance of antitumor immunity, and the inhibition of steroid biosynthesis pathway is sufficient to restore antitumor immunity[26]. Here, the specifically up-regulated steroid biosynthesis pathway here may potentially help tumor cells escape although not in T helper cells. Besides, The specific high expression of CXCL13- CXCR5 in PD1 + CD4 + T cell in tumor tissues may be associated with worse tumor prognosis as previous studies reported that CXCL13-CXCR5 promoted tumor progression, invasion and metastasis through non cancerous tumors in the tumor microenvironment[37].

Intercellular interaction analyses based on ligand-receptor pairs revealed malignant cells interact with CAFs via the MDK-NCL pathway. Previous literature of the interaction between MDK and NCL mainly focus on immunosuppression. MDK was also found to promote articular chondrocyte proliferation through the MDK-LRP1-NCL signaling pathway[38]. Therefore, we hypothesized that the MDK in esophageal cancer cell could interact with NCL on the surface of CAFs to upregulate the proliferation of CAFs. CAF-mediated control of tumor progression include mesenchymal-dependent and mesenchymal-independent mechnisms. The latter facilitates cancer cells invasion of ECM by co-migration or ECM remodeling thus favoring their metastatic potential[39]. Notably, the enriched MDK-NCL signal was observed in two specific subclusters of CAFs. mCAF1 was related to ECM organization and eCAF was associated with energy metabolism and EMT. Although the abundance of these two subclusters was not increased in human intramucosal ESCC specimen compared to paratumor tissue, the highly upregulated MDK-NCL pathway in interaction with E7 cells compared with the interactions with other epithelial cell clusters was negligible. IHC further confirmed the gradual increase of MDK and NCL in high grade dysplasia, intramucosal ESCC, and progressive ESCC. Therefore, the enriched MDK-NCL signal could serve as a sign of CAF activation to stimulate downstream pathways for facilitating tumor invasion, and therefore might be a potential early biomarker of ESCC progression.

Limitations of our study should also be taken into considerations when interpreting the results. First, the limited sample size may lead to the bias of our results. Second, the scarcity of the early ESCC samples brought difficulty in carrying out validation experiments on some specific clusters. Nevertheless, through the above efforts, we believe that our study will contribute to the comprehension of the TME and cellular heterogeneity in both early and progressive ESCC patients and will serve as a valuable resource for in-depth exploration of the pathogenesis of ESCC and identification of the potential therapeutic targets for early ESCC in the future.

Conclusions

In conclusion, we present the cellular atlas of human intramucosal ESCC, and pinpointed the changes of cell subsets and transcriptional levels related to initiation and development of early ESCC in the tumor microenvironment. These findings provide unique insights for development of novel biomarkers and intervention of ESCC.

Abbreviations

CAFs, cancer-associated fibroblasts; CNV, copy number variation; DC, dendritic cells; ESCC, esophageal squamous cell carcinoma; ESD, endoscopic submucosal resection; GEPIA, Gene Expression Profiling Interactive Analysis; GO, Gene Ontology; HE, hematoxylin-eosin; IHC, immunohistochemistry.MM, monocyte/macrophage; PBMC, peripheral blood mononuclear cells; tSNE, t-distributed stochastic neighbor embedding;

Declarations

Ethical Approval and Consent to participate

Approval for this study was issued by the Ethics Committee of Zhongshan Hospital, Fudan University, China. Informed consent was obtained from each patient.

Consent for publication

Not applicable

Availability of supporting data

All data generated or analysed during this study are included in this published article [and its supplementary information files].

Competing interests

The authors declare that they have no competing interests.

Funding

This study was supported by grants from Shanghai Municipal Health Commission, Collaborative Innovation Cluster Project(2019CXJQ02)[establishing the design of the study and responsible for sequencing], National Natural Science Foundation of China (82003074 and 82172787) [responsible for collection, analysis and validation of the data]. Chen Guang Program of Shanghai Municipal Education Committee (18CG07) [responsible for collection, analysis and validation of the data], and Shanghai "Rising Stars of Medical Talent" Youth Development Program(Youth Medical Talents – Specialist Program SHWJRS(2021)-99) [responsible for collection, analysis and validation of the data].

Author's contributions

L. XY, L. YB and X. JC drafted the original manuscript and visualized the data. Z. YF, Z. Y and Z. JW analyzed and visualized the data. R. YY, W. LF, H. JW, Z. Z, H. MJ, C. TY and X. XY helped with the access of resources. Z. PH and Z. YQ were responsible for the conceptualization, supervision and review&editing of the manuscript. All authors read and approved the final manuscript.

Acknowledgements

Not applicable

Authors' information

Not applicable

References

1. Sung H, Ferlay J, Siegel RL, et al. Global Cancer Statistics 2020: GLOBOCAN Estimates of Incidence and Mortality Worldwide for 36 Cancers in 185 Countries. CA Cancer J Clin 2021;71:209–249.
2. Lin Y, Totsuka Y, He Y, et al. Epidemiology of esophageal cancer in Japan and China. J Epidemiol 2013;23:233–42.
3. Zhang Y, Ding H, Chen T, et al. Outcomes of Endoscopic Submucosal Dissection vs Esophagectomy for T1 Esophageal Squamous Cell Carcinoma in a Real-World Cohort. Clin Gastroenterol Hepatol 2019;17:73–81.e3.
4. Oppedijk V, van der Gaast A, van Lanschot JJ, et al. Patterns of recurrence after surgery alone versus preoperative chemoradiotherapy and surgery in the CROSS trials. J Clin Oncol 2014;32:385–91.
5. Berry MF. Esophageal cancer: staging system and guidelines for staging and treatment. J Thorac Dis 2014;6 Suppl 3:S289-97.
6. Kitagawa Y, Uno T, Oyama T, et al. Esophageal cancer practice guidelines 2017 edited by the Japan Esophageal Society: part 1. Esophagus 2019;16:1–24.
7. Song Y, Li L, Ou Y, et al. Identification of genomic alterations in oesophageal squamous cell cancer. Nature 2014;509:91–5.
8. Zheng Y, Chen Z, Han Y, et al. Immune suppressive landscape in the human esophageal squamous cell carcinoma microenvironment. Nat Commun 2020;11:6268.
9. Yao J, Cui Q, Fan W, et al. Single-cell transcriptomic analysis in a mouse model deciphers cell transition states in the multistep development of esophageal cancer. Nat Commun 2020;11:3715.
10. Inoue H, Rey JF, Lightdale C. Lugol chromoendoscopy for esophageal squamous cell cancer. Endoscopy 2001;33:75–9.
11. Shimizu Y, Omori T, Yokoyama A, et al. Endoscopic diagnosis of early squamous neoplasia of the esophagus with iodine staining: high-grade intra-epithelial neoplasia turns pink within a few minutes. J Gastroenterol Hepatol 2008;23:546–50.
12. Guo W, Wang D, Wang S, et al. scCancer: a package for automated processing of single-cell RNA-seq data in cancer. Brief Bioinform 2021;22.
13. Müller S, Liu SJ, Di Lullo E, et al. Single-cell sequencing maps gene expression to mutational phylogenies in PDGF- and EGF-driven gliomas. Mol Syst Biol 2016;12:889.
14. Patel AP, Tirosh I, Trombetta JJ, et al. Single-cell RNA-seq highlights intratumoral heterogeneity in primary glioblastoma. Science 2014;344:1396–401.
15. Wu Y, Yang S, Ma J, et al. Spatiotemporal Immune Landscape of Colorectal Cancer Liver Metastasis at Single-Cell Level. Cancer Discov 2022;12:134–153.
16. Yu G, Wang LG, Han Y, et al. clusterProfiler: an R package for comparing biological themes among gene clusters. Omics 2012;16:284–7.

17. Jin S, Guerrero-Juarez CF, Zhang L, et al. Inference and analysis of cell-cell communication using CellChat. Nat Commun 2021;12:1088.
18. Wang Y, Wang R, Zhang S, et al. iTALK: an R Package to Characterize and Illustrate Intercellular Communication. 2019:507871.
19. Griss J, Bauer W, Wagner C, et al. B cells sustain inflammation and predict response to immune checkpoint blockade in human melanoma. Nat Commun 2019;10:4186.
20. Park JH, Pyun WY, Park HW. Cancer Metabolism: Phenotype, Signaling and Therapeutic Targets. Cells 2020;9.
21. Chen Z, Zhao M, Liang J, et al. Dissecting the single-cell transcriptome network underlying esophagus non-malignant tissues and esophageal squamous cell carcinoma. EBioMedicine 2021;69:103459.
22. Ogretmen B. Sphingolipid metabolism in cancer signalling and therapy. Nat Rev Cancer 2018;18:33–50.
23. Dinh HQ, Pan F, Wang G, et al. Integrated single-cell transcriptome analysis reveals heterogeneity of esophageal squamous cell carcinoma microenvironment. Nat Commun 2021;12:7335.
24. Zheng L, Qin S, Si W, et al. Pan-cancer single-cell landscape of tumor-infiltrating T cells. Science 2021;374:abe6474.
25. Makowski L, Chaib M, Rathmell JC. Immunometabolism: From basic mechanisms to translation. Immunol Rev 2020;295:5–14.
26. Mahata B, Pramanik J, van der Weyden L, et al. Tumors induce de novo steroid biosynthesis in T cells to evade immunity. Nat Commun 2020;11:3588.
27. Buck MD, O'Sullivan D, Klein Geltink RI, et al. Mitochondrial Dynamics Controls T Cell Fate through Metabolic Programming. Cell 2016;166:63–76.
28. Liu X, Arfman T, Wichapong K, et al. PAD4 takes charge during neutrophil activation: Impact of PAD4 mediated NET formation on immune-mediated disease. J Thromb Haemost 2021;19:1607–1617.
29. Kanao H, Enomoto T, Kimura T, et al. Overexpression of LAMP3/TSC403/DC-LAMP promotes metastasis in uterine cervical cancer. Cancer Res 2005;65:8640–5.
30. Szpor J, Streb J, Glajcar A, et al. Dendritic Cells Are Associated with Prognosis and Survival in Breast Cancer. Diagnostics (Basel) 2021;11.
31. Chen Z, Zhou L, Liu L, et al. Single-cell RNA sequencing highlights the role of inflammatory cancer-associated fibroblasts in bladder urothelial carcinoma. Nat Commun 2020;11:5077.
32. Zhang Q, He Y, Luo N, et al. Landscape and Dynamics of Single Immune Cells in Hepatocellular Carcinoma. Cell 2019;179:829–845.e20.
33. Gong J, Lin Y, Zhang H, et al. Reprogramming of lipid metabolism in cancer-associated fibroblasts potentiates migration of colorectal cancer cells. Cell Death Dis 2020;11:267.
34. Affo S, Nair A, Brundu F, et al. Promotion of cholangiocarcinoma growth by diverse cancer-associated fibroblast subpopulations. Cancer Cell 2021;39:866–882.e11.

35. Bartoschek M, Oskolkov N, Bocci M, et al. Spatially and functionally distinct subclasses of breast cancer-associated fibroblasts revealed by single cell RNA sequencing. Nat Commun 2018;9:5150.
36. Kroemer G, Pouyssegur J. Tumor cell metabolism: cancer's Achilles' heel. Cancer Cell 2008;13:472–82.
37. Hussain M, Liu J, Wang GZ, et al. CXCL13 Signaling in the Tumor Microenvironment. Adv Exp Med Biol 2021;1302:71–90.
38. Deng Q, Yu X, Deng S, et al. Midkine promotes articular chondrocyte proliferation through the MK-LRP1-nucleolin signaling pathway. Cell Signal 2020;65:109423.
39. Fiori ME, Di Franco S, Villanova L, et al. Cancer-associated fibroblasts as abettors of tumor progression at the crossroads of EMT and therapy resistance. Mol Cancer 2019;18:70.

Figures

Figure 1

scRNA-Seq profiling of the human intramucosal ESCC microenvironment

A. Workflow depicting sample collection, single cell preparation, and RNA-seq.

B. t-SNE plot displaying main cell types in human intramucosal ESCC microenvironment.

C. Bubblemap displaying the top 10 SDE genes in each cell type, both color and size indicate the effect size.

D. Distribution of cells in different specimens

E. Distribution of cells in different patients

F. B cell percentage in early and progressive ESCC patients (** indicates a P value < 0.01)

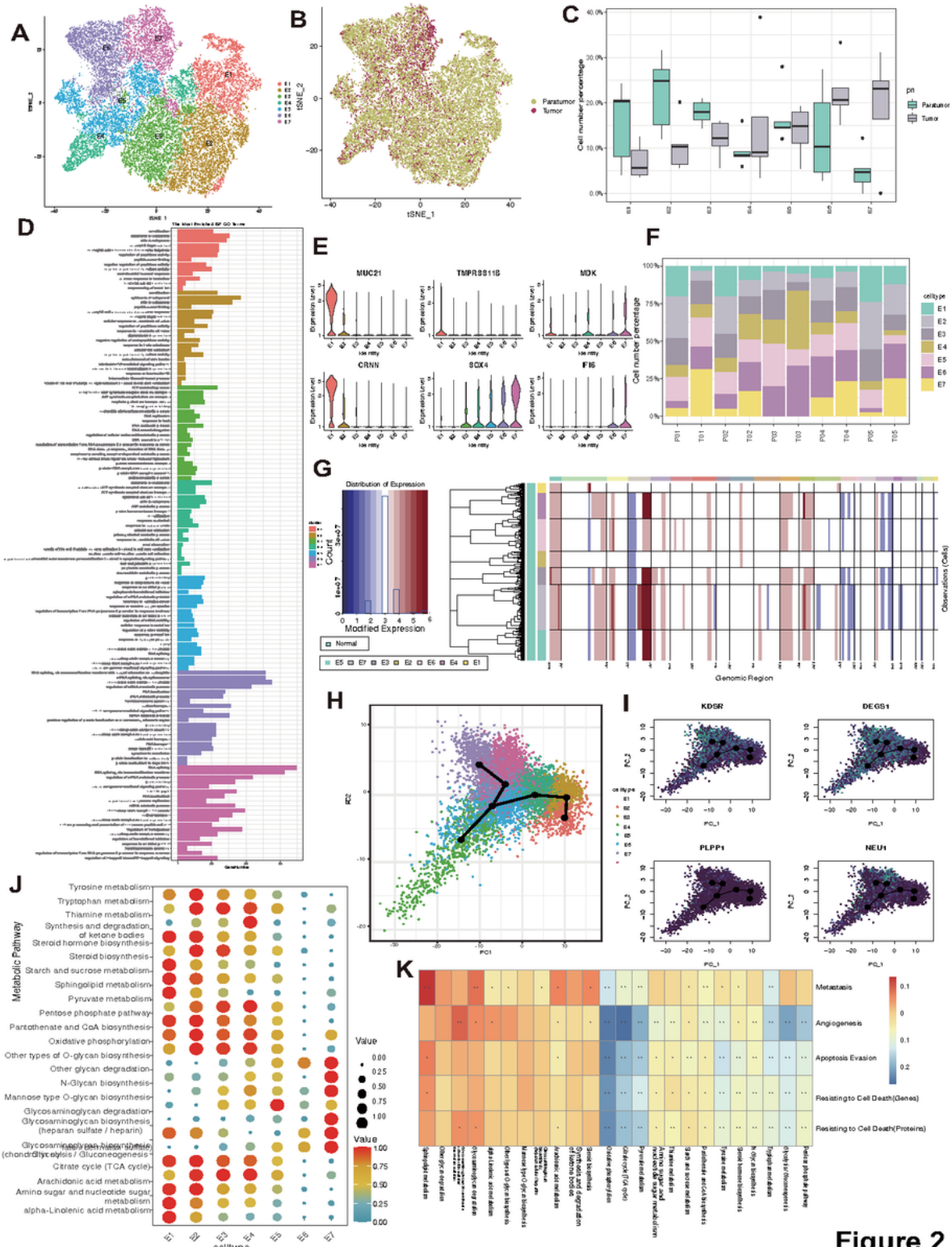

Figure 2

Figure 2

The single-cell transcriptomes of epithelial cells in human intramucosal ESCC.

A. t-SNE plot revealing the 7 epithelial cell subclusters.

B. Distribution of epithelial cells in paratumor and tumor specimen revealed by t-SNE plot.

C. Cell number percentage of 7 subclusters in different specimen.

D. GO analysis for E1~E7 subclusters.

E. Violin plot showing important markers of E1~E7 subclusters.

F. Distribution of 7 subclusters in different patients, with E7 absent in patient 3.

G. CNV profiles showing a relative variation between epithelial cells originated from tumor and paratumor specimen after Bayes normalization.

H. Psudotome analysis revealing trajectory paths of intramucosal ESCC initiation.

I. t-SNE plot showing gene expression in sphingolipid metabolism pathways of E7 subcluster.

J. Dotplot showing metabolic characteristics of 7subclusters, both color and size indicate the effect size.

K. Correlation between the 24 representing metabolic pathways and phenotypic scores of E7 subcluster (* indicates a P value < 0.05 and ** <0.01).

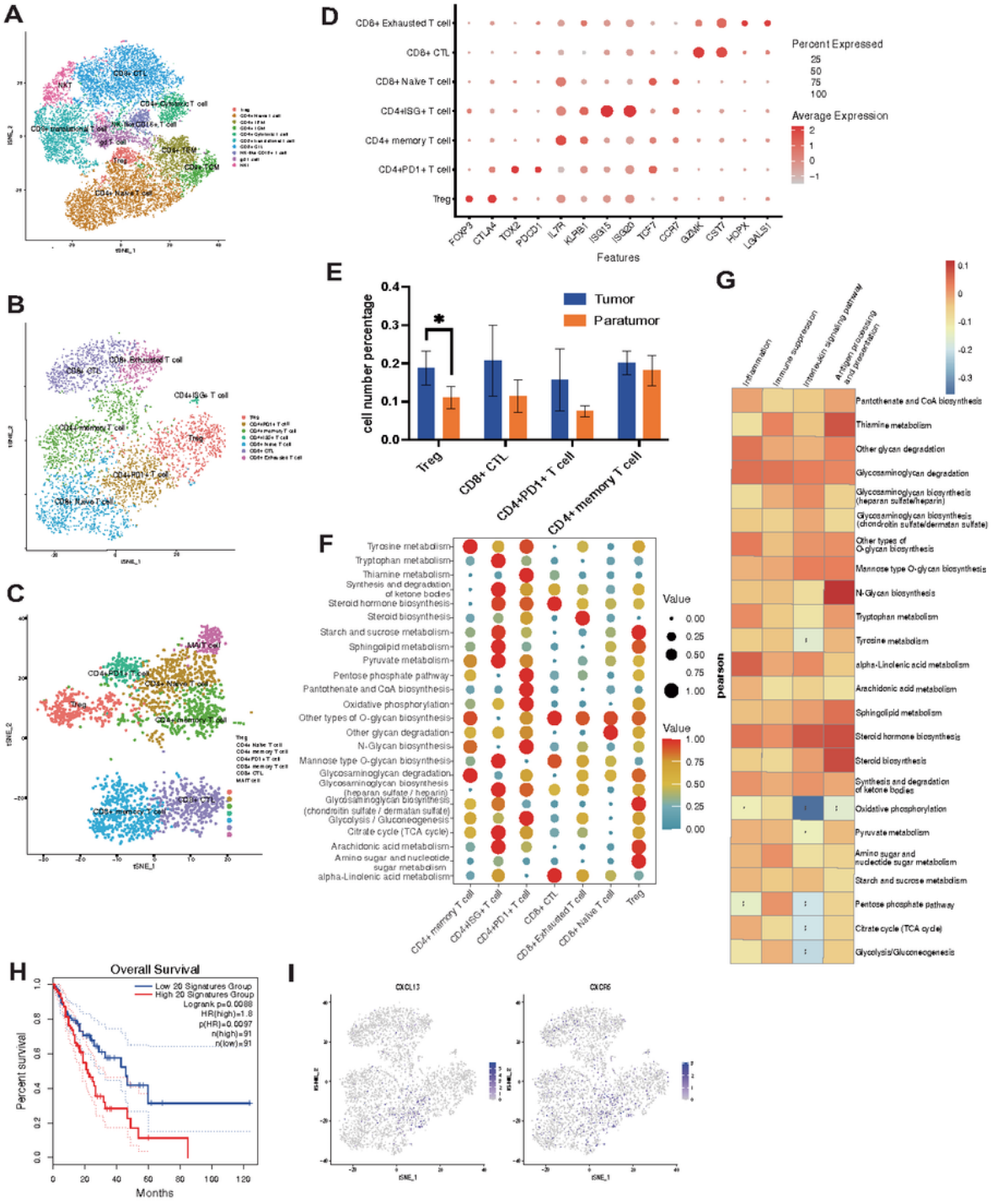

Figure 3

Figure 3

Exhausted T cells and suppressive immune microenvironment in human intramucosal ESCC

A,B,C.t-SNE plots revealing T cell subclusters in PBMC(A), tumor specimen s(B) and paratumor specimens(C).

D. Dotplot showing important markers of T cell subclusters, both color and size indicate the effect size.

E. Distribution of T cell subclusters in different specimens (* indicates a P value < 0.05).

F. Dotplot showing the score of 24 representative active metabolic pathways using scmetabolism in all T cell clusters, both color and size indicate the effect size.

G. Correlation between classical phenotype scores of T cells and the 24 representing metabolic pathways(* indicates a P value < 0.05 and ** <0.01).

H. Kaplan-Meier analysis showing overall survival of the top 20 PD1+CD4+ T cells markers in ESCC patients.

I. CXCL13 and CXCR5 expression in PD1+CD4+T cells shown by tSNE plots.

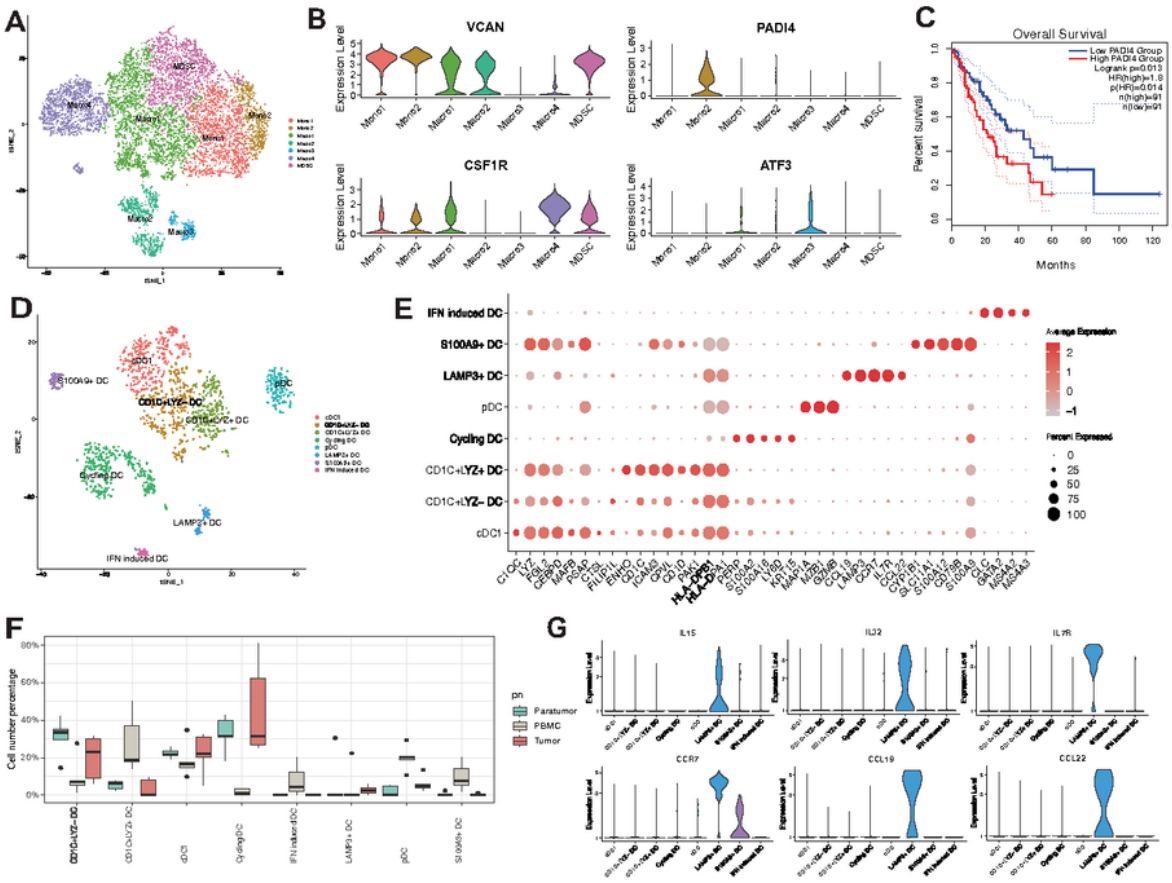

Figure 4

Figure 4

Characterization of myeloid cell subpopulations.

A. t-SNE plot showing 7 monocyte/macrophage cell subclusters.

B. Violin plots showing gene signatures of MM cell subclusters.

C. Kaplan-Meier analysis showing overall survival of PADI4 in ESCC patients.

D. t-SNE plot showing dentric cell subclusters.

E. heatmap showing important gene signatures of DC subclusters.

F. Distribution of DC subclusters in different specimens.

G. Violin plots showing immune-relevant genes expressed by LAMP3+ DCs.

F. cell number percentage in different specimens.

Figure 5

Distinct fibroblast subpopulations in human intramucosal ESCC ecosystem.

A. t-SNE plotshowing 5 subclusters of cancer associated fibroblasts.

B. Violin plot showing important gene signatures expressed by all the 5 CAF subclusters collectively.

C. Dotplot showing important gene signatures of CAF subclusters respectively, both color and size indicate the effect size.

D. GO analysis for CAF subclusters.

E. Distribution of CAF subcusters in different specimens.

F. GO analysis for CAF derived from tumor and paratumor specimens.

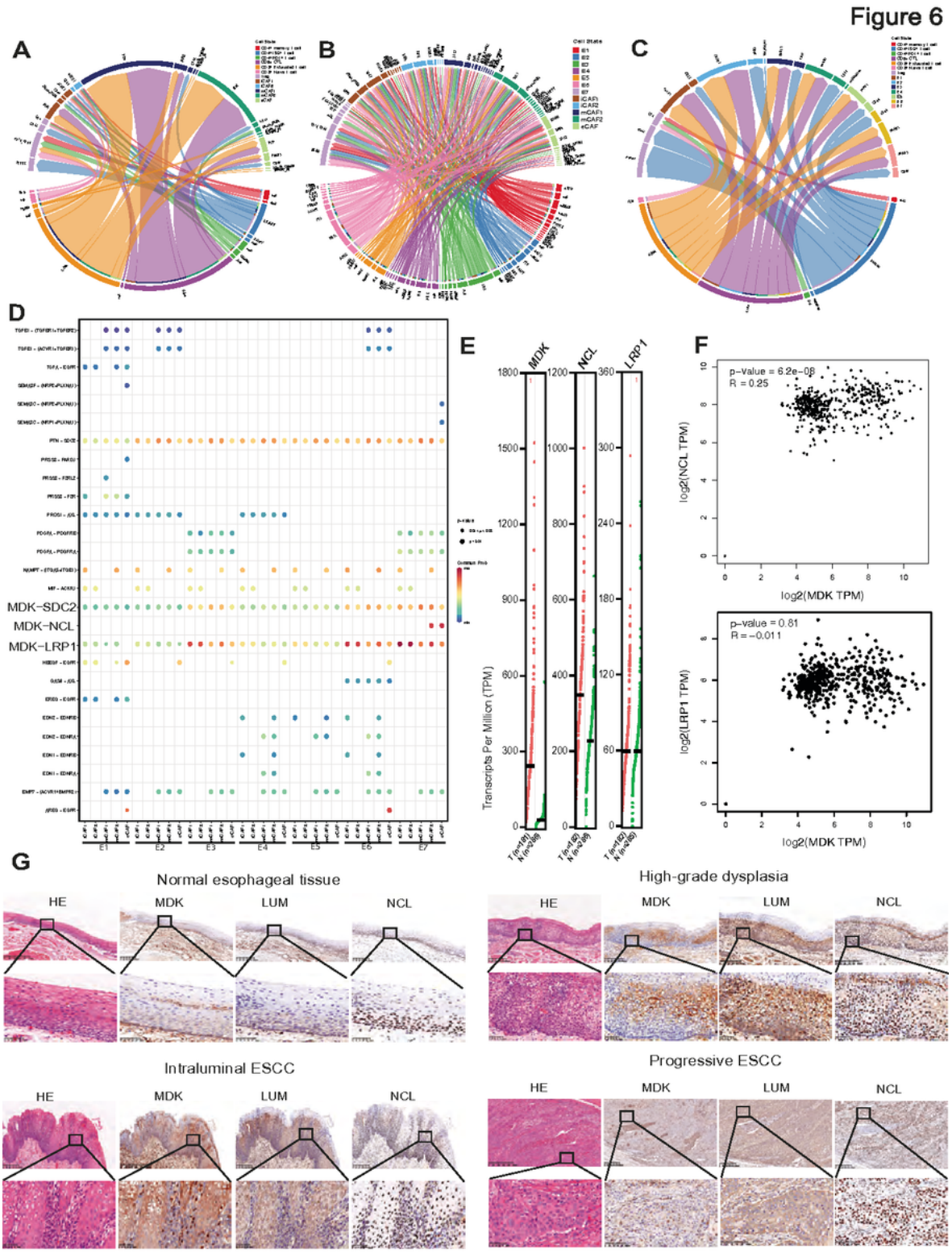

Figure 6

Altered crosstalk between subclusters in human intramucosal ESCC.

A. circos plots showing crosstalk between T cell and CAF subclusters.

B. circos plots showing crosstalk between epithelial cells and CAF subclusters.

C. circos plots showing crosstalk between T cell and epithelial cell subclusters.

D. dotplot showing upregulated and downregulated interactions between epithelial cells and CAF subclusters.

E. expression level of MDK, NCL and LRP1 in human esophageal cancer and paratumor specimen, data from GEPIA.

F. correlation analyses between MDK and NCL, and between MDK and LRP1, data from GEPIA.

G. HE staining and IHC in ESCC specimen of paratumor specimen, high grade intraepithelial neoplasia, intramucosal ESCC and progressive ESCC.

Supplementary Files

This is a list of supplementary files associated with this preprint. Click to download.

- Supplementaryfigure1.pdf
- Supplementaryfigure2.pdf
- Supplementaryfigure3.pdf
- Supplementaryfigure4.pdf
- Supplementaryfigure5.pdf
- Supplementarymaterialsandtables.pdf